PAPER • **OPEN ACCESS**

Effects of carbon dioxide dilution and composition on tip opening and OH radical distribution in laminar non-premixed Bunsen flame

To cite this article: Zhonghua Wang *et al* 2019 *IOP Conf. Ser.: Earth Environ. Sci.* **267** 032026

Effects of carbon dioxide dilution and composition on tip opening and OH radical distribution in laminar non-premixed Bunsen flame

Zhonghua Wang[1], Qiang Tang[1], Zhongqing Yang[1] and Keliang Li[1]

[1]Key Laboratory of Low-grade Energy Utilization Technologies and Systems, Chongqing University, Ministry of Education, Chongqing 400030, PR China

tangqiang@cqu.edu.cn

Abstract: Effects of CO_2 dilution and composition on tip opening and flame OH radical distribution in laminar non-premixed Bunsen flame were investigated by using planar laser induced fluorescence (PLIF) technique. Experiments were conducted at different component fractions diluted with CO_2 at 20%, 25%, and 30%. The syngas were produced by biomass catalytic gasifying. Stretch rates were calculated and combined with OH-PLIF images and simulation. We conducted kinetic simulation to analyze the production of OH radical. Results show that as V_{H2} increases and hydrogen slightly increases, the effect of mass diffusion is enhanced , in addition, the value of stretch rate decreases, and the tip opening becomes further obvious. The profile of OH radical distribution also becomes broad. Finally, the total production rates of OH radicals increases with a rate less than 7.5%. Hence, the maximum value of OH radical counts is reduced by 33.33%, 27.92%, and 23.09%. Nonetheless, with the increasing addition of CO_2, the effect of mass diffusion is weakened; besides, chemical reaction residence time increases, and the value of stretch rate increases; the tip opening is less obvious. Although the distribution area of OH was narrowed, its production decreased and the relative concentration of all OH radical decreased.

1. Introduction

In general, fossil energy reserves are limited and cause serious pollution problems, Therefore, substitute energy is urgently needed. Hydrogen energy is a potential energy to solve this problem due to its clean emissions, high efficiency and reproducibility[1]. Biomass energy is widely distributed and easily acquired. It is also a low-cost and appropriate carrier of hydrogen energy. Up to now, in the field of hydrogen production from biomass pyrolysis, different kinds of biomass materials, reactors, catalysts, and reaction parameters settings have been researched to raise the output of hydrogen,[2, 3] Meanwhile, the biomass gasifying technology has gathered further attention because of its promotion in hydrogen gas production[4, 5]. In summary, V_{H2} can reach up to 50% for biomass pyrolysis, and V_{H2} increases to 60% when biomass gasifying technology is applied. Moreover, V_{CO2} is approximately 25 % (±%5).

High calorific value gas with large volume fraction of hydrogen is the greatest strength of biomass gasifying technology. On this basis, syngas from biomass by catalytic steam gasification can be applied to gas turbines.[6] Moreover, previous studies have focused on CO/H_2 or CH_4/H_2. However, little attention has been devoted to syngas, which is consist of multiple gases. Therefore, syngas non-premixed combustion should be researched.

Owing to the high sensibility, short response time and small interference of the planar laser induced

fluorescence (PLIF) technology, accurate data are obtained when conducting experiments. Therefore PLIF technology has become a hot spot in combustion researches[7, 8].The burning velocity of syngas-type fuels have been measured by different methods, such as Heat flux method[9] and Bunsen flame method[10]. These methods pay much attention on equivalence ratio and CO_2/N_2 dilution.[11-13] Besides, others are focused on OH distributions[14]. The flame structure of syngas combustion has been intensively researched. Fu et al.[15] conducted experiments on laminar flame structure of syngas for X_{H2} ranging from 20% to 100% and equivalence ranging from 0.5 to 1.8. Tu et al.[16] studied the laminar flame structure with different X_{H2} at equivalence of 1.0, their results showed that as the X_{H2} increases up to 40%, the shape of the flame structure resemble a "W". Wang et al.[17] studied stretch and preferential diffusion on tip opening, their result showed that the tip opening is enhanced as the equivalence decreases, and the hydrogen fraction and the Reynolds number increase. Tran et al.[18] studied the tip openings in Bunsen flames, their results showed that the tip opening occurs at a constant equivalence ration.

The present study aims to focus on the effects of components fraction, CO_2 dilution on tip opening and OH radical distribution of laminar non-premixed Bunsen flames by using OH-PLIF technology. The measurement of laminar non-premixed syngas Bunsen flames will be conducted at different components fractions varying from 20% to 65% for hydrogen, 10% to 40% for carbon monoxide, 3% to 15% for methane, and 20%, 25% and 30% for CO_2 dilutions. Moreover, the velocity vector of the flow at different conditions will be numerically simulated using FLUENT 6.3.26. we will calculate stretch rates quantitatively to analyze the effect of components fractions and CO_2 dilutions on tip opening by using the experiment data and numerical simulation data. The distribution of OH radicals will be discussed by using the OH-PLIF images subtracted with background noise and corrected with the laser beam profile.

2. Experimental setup and procedures

2.1 Experimental apparatus

The non-premixed Bunsen flame was measured using Planar Laser Induced Fluorescence (PLIF) technique. The experimental apparatus includes three parts: OH-PLIF system, gas supply system and laminar non-premixed Bunsen burner. The OH-PLIF system consists of a laser source, that comprises an Nd: YAG laser as a pump laser, a tunable dye laser, a set of reflecting mirrors and optical lens, equipment for the fluorescence signal detection and data acquisition and software.

The wavelength of 355 nm light from the YAG laser was used to pump a dye laser, the dye laser generated 567.110 nm light, which was then doubled to 283.555 nm UV light by a double frequency crystal. The laser is used to excite the OH base transition and form a 50 mm high and 0.8 mm thick sheet through the flame center after passing through the lens group. OH fluorescence signal is received by ICCD camera (LAVISION, VC14-0120) with UV lens (UV-60 mm, F3.5s), a filter LIF for OH (LAVISION, VZ14-0353). The maximum energy of a single laser shot was about 13 mJ. The length of the object that the ICCD camera records is calibrated by a graduated plate with the system software Davis 8. The gate and delay of the ICCD camera are set to 100 ns and 60 ns, respectively, for minimizing the effects of ambient lights. The gain of the intensifier was increased to 60% to optimize the captured fluorescence signals. The schematic of the experimental system is shown in Fig. 1.

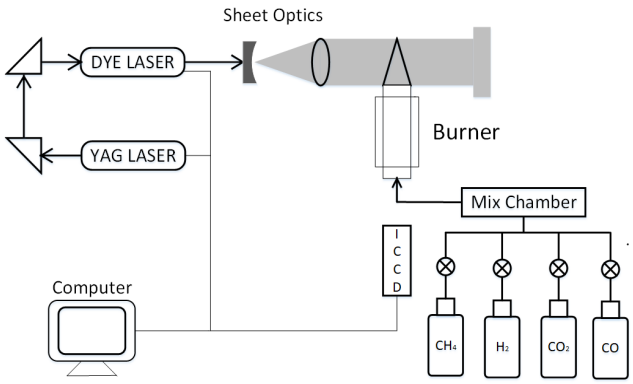

Figure 1. Schematic of OH-PLIF and gas delivery system

H_2/CO/CH_4 mixtures with CO_2 dilution were tested in this study. The experiment was operated at atmospheric pressure, room temperature and Reynolds number equals 2000. The purity of H_2, CO, and CH_4 were over 99.99%. V_{H2} (V_{CO}, V_{CH4}) is the volume fraction of H_2 (CO, CH_4) in the syngas fuel. Similarly, V_{CO2} is used as the CO_2 volume fraction in the syngas fuel. The volume flow of each gas was controlled by flow meters. Then, it was mixed in a stainless chamber before entering the burner. The diameter and length of Bunsen burner is 5 mm and a length of 26 cm, respectively.

Table 1. Fuel composition

Fuel	V_{CH4}/ (%)	V_{H2}/ (%)	V_{CO}/ (%)	V_{CO2}/ (%)	hydrogen content/ per mole gas (mol)
A1	15.7	25.0	39.3	20.0	1.10
A2	12.8	35.0	32.1	20.0	1.22
A3	10.0	45.0	25.0	20.0	1.24
A4	8.3	51.0	20.7	20.0	1.32
A5	7.1	55.0	17.9	20.0	1.42
A6	4.3	65.0	10.7	20.0	1.44
B1	14.7	23.4	36.8	25.0	1.03
B2	12.1	32.8	30.1	25.0	1.14
B3	9.4	42.2	23.4	25.0	1.16
B4	7.8	47.8	19.4	25.0	1.24
B5	6.7	51.6	16.7	25.0	1.33
B6	4.0	60.9	10.0	25.0	1.35
C1	13.8	21.9	34.4	30.0	0.96
C2	11.3	30.6	28.1	30.0	1.07
C3	8.8	39.4	21.9	30.0	1.09
C4	7.3	44.6	18.1	30.0	1.16
C5	6.3	48.1	15.6	30.0	1.24
C6	3.8	56.9	9.4	30.0	1.26

2.2 Experiment method

The syngas studied in this experiment is a mixture of simplifications of gases such as C_2H_2 and C_2H_4 which have been verified by related literature [19-21] and negligible amounts of other components are not considered.

According to the relevant data, the CO_2 stays at 20%-30%,furthermore some other gas such as ethane, or ethylene takes a small account. We simplified these data into three groups (A-B-C), the CO_2 dilution rate is at 20%, 25%, and 30%. (see Table 1.) From A1 to A6, V_{H2} increased, V_{CO2} remained at 20%; moreover, the relative contents of CH_4 and CO remained as 2.5, and the hydrogen content increased slightly. From A1-B1-C1, V_{CO2} gradually increased, whereas the other relative contents remained basically unchanged(1/1.6/2.5).

The FLUENT 6.3.26 is used to calculate the velocity vector of the flow at atmospheric pressure and room temperature. Regardingr the material, the syngas was defined according to Table .1, and the

relevant settings refer to the research of Wang et al. GRI3.0 kinetic mechanism and OPPDIF model is used to calculate the production rates of OH radicals and the normalized sensitivity coefficient on dominants reactions by Chemkin-pro software. Related settings are used as reference for analyzing the OH radical distribution.[22] To be synchronous with the experimental results, simulation conditions are made in consistent with the experimental conditions.

2.3 Data processing method

For each condition, 200 instantaneous OH-PLIF images were processed for statistical analysis. The images were subtracted with background noise and corrected with the laser beam profile. The OH concentration and the reaction zone indicated by OH were seen from the OH-PLIF images. The flame front structure were also seen.

The stretch rate is an important parameter closely related to the local combustion characteristics of the flame. The OH-PLIF image processing minimized other effects, therefore, the flame obtained in the experiment was a stable flame surface. The expression for the stretch rate κ is as follows:[17]

$$\kappa = -n \cdot \nabla \times (v_s \times n) \tag{1}$$

The OH-PLIF images proved that the OH profile was almost symmetrical. The left side was chosen for analysis. On the basis of the OH-PLIF images, the polynomial of the two dimensional flame front surface can be expressed by f(x),and n is defined as normal vector at the flame front，and v_s is defined as unburned syngas velocity vector(flow velocity vector). By substituting the vector v_s and n into Eq.(1), the stretch rate can be expressed as：

$$\kappa = \frac{\frac{\partial u}{\partial x} + \frac{df(x)}{dx}\{\frac{\partial u}{\partial y} + \frac{\partial v}{\partial x}\} + \{\frac{df(x)}{dx}\}^2 \frac{\partial v}{\partial y}}{\{\frac{df(x)}{dx}\}^2 + 1} + \frac{\frac{d^2 f(x)}{dx^2}}{[\{\frac{df(x)}{dx}\}^2 + 1]^{3/2}} \frac{v - u\frac{df(x)}{dx}}{[\{\frac{df(x)}{dx}\}^2 + 1]^{1/2}} \tag{2}$$

The first and second terms of the equation indicated the effect of flow strain and the flame curvature to the stretch rate. They can be presentedt as κ_s and κ_c, respectively. The effect of κ to the flame tip opening, the OH concentration and the reaction zone indicated by OH will be discussed in the study.

The data processing of the stretch rate are as follows. In accordance with the OH-PLIF images, over 50 coordinate points on the flame front surface were used to fit a polynomial expressed as f(x). Then the data df(x)/dx and $d^2f(x)/dx^2$ in Eq. (2) could be directly calculated. The data u and v of the 50 coordinate points are obtained from a simulation. Two polynomials, namely, u(x, y) and v(x, y) were obtained. Then, the data of $u, v, \partial u/\partial x, \partial u/\partial y, \partial v/\partial x, \partial v/\partial y$ could be obtained. The stretch rate was calculated by substituting the data calculated above into Eq. (2).

3. Results and discussions

3.1 Effect of hydrogen components fractions on tip opening

Fig.2 shows that the OH-PLIF images varied from components fractions, as the conditions A1 to A6 show in Table.1.These images also proved that OH concentration was almost zero at the tip of the flame, and the OH regions were distributed on both side of the syngas flow independently. OH radicals are important intermediate products of combustion, it is used to represent the reaction zone; it indicates that the combustion intensity is nearly zero at the tip of the flame and tip opening phenomenon is happened. What's more, from condition A1 to A6, the tip opening becomes more obvious. And the OH-PLIF images of conditions B1-B6 (C1-C6) present the same situation when compared to A1-A6. The effect of components fraction on tip opening will be analyzed quantitatively by calculating the stretch rates.

Fig. 3 showed that stretch rates varied from different components fractions. The graphics were

created by utilizing Origin85. The origin of coordinates is the center of the tube where the syngas comes. H is the height above the burner outlet. Fig. 3(a) shows that κ is negative at the beginning, with the increase in H, κ increases sharply, and the κ of condition A6 shows the fastest growth rate. κ becomes gentle at the position near H=30 mm, κ remains stable at H=30~70 mm at a value at approximately -7 s^{-1}, and then shows a decreasing trend. From condition A1 to A6, the absolute value of κ increases at H=0~30 mm, whereas κ is almost the same at H=30~70 mm. The κ of condition A6 shows a decreasing trend first, whereas the κ of condition A1 is the last when continuously increasing H.

The values of κ_s are shown in Fig. 3(b). The figure shows the same variation trend as κ, and the value is almost equal to κ, indicating that the effect of flow strain plays a leading role to the variation of κ. Moreover, from condition A1 to A6, the value of κ_s decreases due to the following reasons: first, the increase in hydrogen content increases the instability of the flame; second, the mass diffusivity increases as the volume fraction of H_2 increases and the volume fractions of CH_4 and CO decrease. As a result, the flow becomes more unstable and the effect of flow strain is enhanced.

The values of κ_c are shown in Fig. 3(c). The figure shows that the values of κ_c are smaller than those of κ; κ_c of A1 at H=30~70 mm is approximately zero. The curvature is approximately zero because the slopes of points κ on the flame front surface are approximate. With the increase in height H, the curvature at the flame tip decreases, thereby resulting in the decrease in κ_c. From A1 to A6, the areas, where κ_c is approximately zero becomes smaller, and the value of κ_c decreases due to the increase in mass diffusivity contributed by H_2. Moreover, as κ_c changes with different component fractions, the approximate shape of the flame front surface changes from “U” to “V”. Moreover, the κ, κ_s, and κ_c of conditions B1–B6 (C1–C6) play the same variation trend when compared with A1–A6.

In summary, from condition A1 to A6 (B1–B6 and C1–C6), the hydrogen content in syngas increases. Consequently, the mass diffusivity increases, and the effect of mass diffusion is enhanced; thus, the tip opening tends to be more evident. From a quantitative angle, the value of κ decreases from A1 to A6 (B1–B6 and C1–C6), the negative stretch at the flame tip is enhanced, and the tip opening becomes more evident consequently.

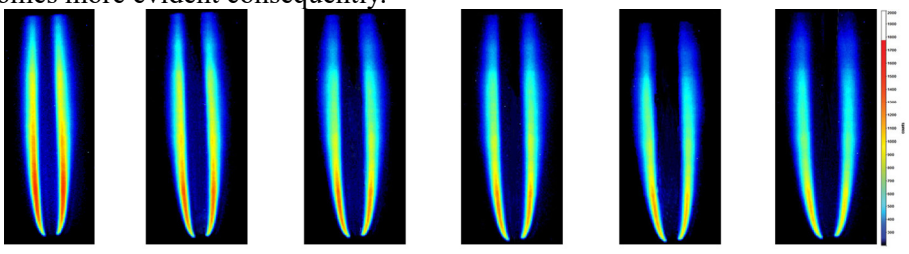

Figure 2. OH-PLIF images of the flames varying with component fractions

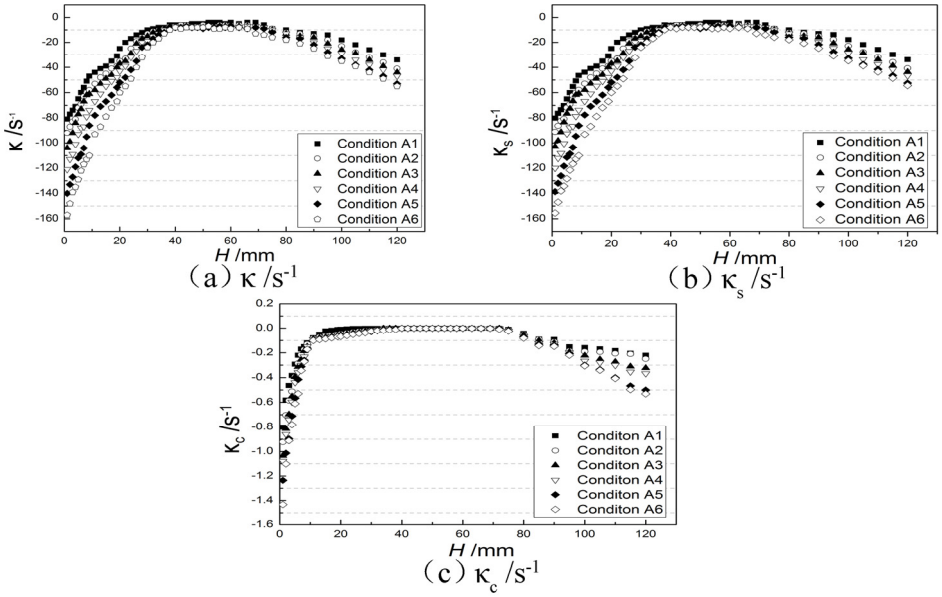

Figure 3. Stretch rates varying with components fractions at 20% CO_2 dilution: (a) stretch rate; (b) stretch rate contributed by flow strain; (c) stretch rate contributed by curvature.

3.2 Effect of CO2 dilution on tip opening

Carbon dioxide and nitrogen are inert gases. In diffusion combustion, the carbon dioxide content of biomass syngas is not fixed, and the nitrogen involved in combustion mostly belongs to the ambient air. However, the nitrogen component in synthesis gas is extremely low, even neglected. Therefore, carbon dioxide has more practical value than nitrogen in the study of the effect of diluted gases on combustion characteristics.

The OH-PLIF images at different CO_2 dilutions are shown in Fig. 4, and conditions A1, B1, and Cl are shown in Table 1. The OH-PLIF images show that the OH profile looks similar to Fig. 2. The opening at the flame tip becomes less evident with the increase in the CO_2 added. The OH-PLIF images of all the other conditions, such as A2, B2, and C2 and A6, B6, and C6 show the same situation as that of A1, B1, and C1. The effect of CO_2 dilution on the tip opening is analyzed quantitatively by calculating the stretch rates.

Fig. 5 shows that the stretch rates vary from CO_2 dilutions at 20%, 25%, and 30%. Fig. 5(a) shows that κ is negative at the beginning, and with the increase in H, κ increases slowly. As the CO_2 addition increases, the height, where κ becomes steady, shifts to the burner outlet. The value of κ fluctuates at -5s^{-1} at H=25~65 mm. With the increasing addition of CO_2, κ of conditions B1 and C1 slightly increases and shows a decreasing trend at a position near H=65 mm. The values of κ_s are shown in Fig. 5(b), which presents the same variation trend as shown in Fig. 3(b). The value of κ_s is approximately the same as that of κ, thereby indicating that the effect of flow strain takes the dominant role. Moreover, the value of κ_s slightly increases with the increase in the added CO_2. The reason is that the mass diffusivity decreases as the volume fraction of H_2 increases. Consequently, the effect of flow strain is weakened. The values of κ_c are shown in Fig .5(c). The figure shows that κ_c is almost equal to zero at H=30~70 mm, and with the increase in CO_2 dilution, the region, where κ_c is approximately zero, becomes larger. The main reason for this phenomenon is the decrease in the hydrogen components as the CO_2 dilution increases. Thus, the effect of mass diffusion decreases and the flame front surface tends to be straight. The κ, κ_s, and κ_c of other controlled trials (such as

A2-B2-C2) present the same variation trend when compared with A1, B1, and C1.

In summary, from condition A1 to B1 to C1 (A2, B2, and C2), the relative content of other components remains unchanged whereas the addition of CO_2 increases. One the one hand, as the volume fraction of carbon dioxide increases, the hydrogen content in syngas decreases, the mass diffusivity decreases, and the effect of mass diffusion is weakened. On the other hand, the temperature decreases as the CO_2 increases, and the chemical reaction residence time increases. Thus, the front surface tend to be more contractive. From a quantitative angle, κ increases from A1 to B1 to C1 (A2, B2, and C2), and the negative stretch at the flame tip is weakened. Thus, the tip opening becomes less evident.

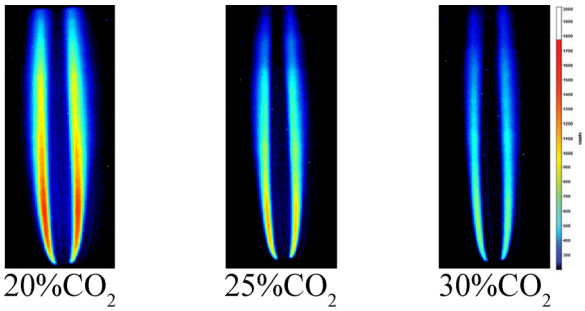

Figure 4. OH-PLIF images of the flames varying from CO_2

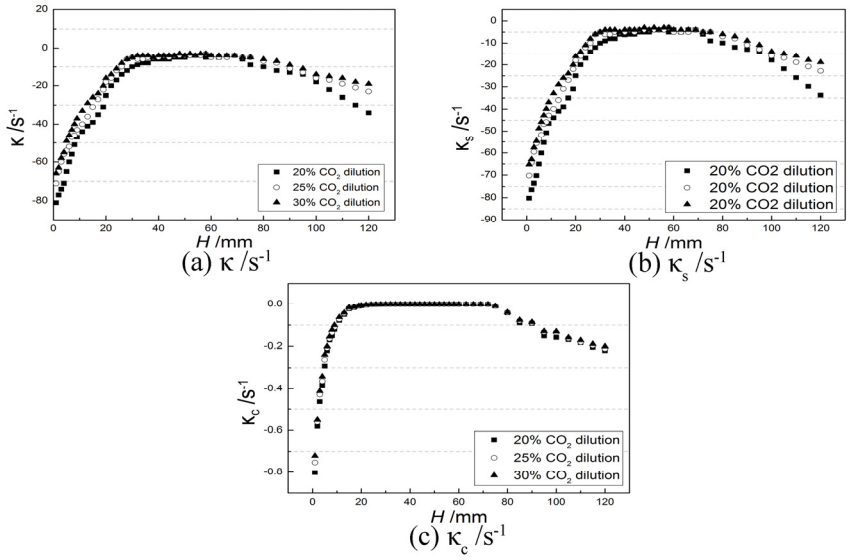

Figure 5. Stretch rates varying from CO_2 dilution: (a) stretch rate; (b) stretch rate contributed by flow strain; (c) stretch rate contributed by curvature.

3.3 Effect of component fraction on flame OH radical distribution

Fig. 2 shows the OH-PLIF images of flames with 20% CO_2 dilution varying from different component fractions, and the conditions A1 to A6 are shown in Table. 1. The OH-PLIF images show that the profile of OH radical distribution becomes broader, and the first image from the left of Fig. 4 is the narrowest, whereas the sixth image is the broadest. The reason is the increase in the hydrogen content from conditions A1 to A6. With the increase in hydrogen content, the effect of diffusion is promoted due to the high mass diffusivity of H_2. As a result, the region, where combustion occurs, becomes broaden.

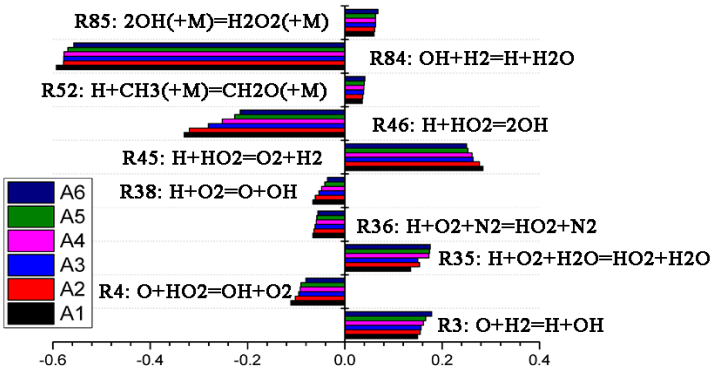

Figure 6. Production rates of OH radicals

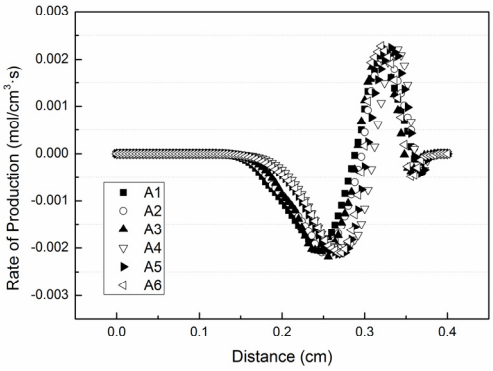

Figure 7. Normalized sensitivity coefficients on dominant reactions at different component fractions

Furthermore, the OH-PLIF images suggest that the maximum value of OH radical counts of condition A1 is 1440 (B1:1026, C1:733). As the condition changes, the value decreases to 960, 740, and 564 with reducing rates of 33.33%, 27.92%, and 23.09% respectively, and the OH radical concentration becomes smaller. The reasons for this phenomenon are as follows: on the one hand, as shown in Table 1 shows, the hydrogen content slightly increases from A1 to A6 (B1–B6, C1–C6). Therefore, the potential production of OH radicals has no evident change. Fig. 6 shows that the total production rates of OH radicals have no evident difference when hydrogen content slightly increases from A1 to A6. Meanwhile, Fig. 8 shows that the peak values of total production rates of OH radicals slightly increase with a rate less than 8%. These findings indicate that the production of OH radicals slightly increases, thereby verifying the previous statement. Moreover, Fig. 7 shows that with the slight increase in hydrogen content, the promotion effect on the reactions of OH production slightly increases (such as R3), and the inhibitory effect on the reactions of OH consumption slightly decreases, thereby verifying the statement once again. One the other hand, the profile of OH radical distribution becomes broader. As a result, the OH radicals are more scattered, and the OH radical concentration becomes smaller. Moreover, conditions B1–B6 (C1–C6) play the same situation when compared with A1–A6.

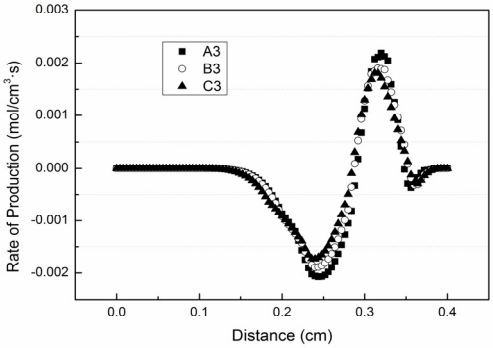

Figure 8. Peak value of total production rates of OH radicals

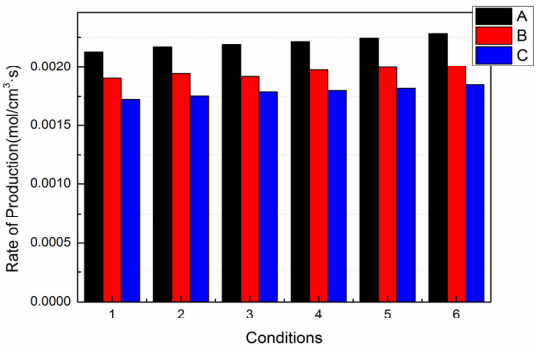

Figure 9. Production rates of OH radicals

Fig. 4 shows OH-PLIF images of flames vary from different CO_2 dilution, as the conditions A1, B1, C1 show in Table. 1. It is figured out from the OH-PLIF images that the maximum value of OH radical counts changes from 1440 to 733, it is reduced by 49.07%, and OH radical concentration shows a decreasing trend, two reasons may contribute to this phenomenon. On the one hand, with the increasing addition of CO_2, the percentage of fuel in syngas decreases and the hydrogen content decreases, as a result, the production of OH radicals decreases, and it is seen from Fig.9 that the total rate of production of OH radicals decrease significantly from condition A3 to B3 to C3 (A1, B1, C1 et al. present the same situation), and it is figured from Fig.8 that the peak values of total production rates of OH radicals decrease a lot with a rate about 20%, these two facts indicate that the production of OH radicals decreases a lot; on the other hand, with the increasing addition of CO_2, the heat capacity increases. As a consequence, the flame temperature reduces, and the production of OH radicals is further reduced consequently. What's more, with the increase of CO_2 dilution, the profile of OH radical distribution becomes narrower. That would be due to the decrease of the flame temperature. As the flame temperature decreases, the burning velocity of flame decreases, as a result, the chemical reaction residence time increases, the OH radicals are more concentrated and the profile of OH radical distribution becomes narrower. The OH-PLIF images of conditions A2, B2, C2 et al. present the same situation when compared to A1, B1, C1, the maximum value of OH radical counts reduced by 41.25%~49.7%.

4. Conclusions

The effect of component fractions and CO_2 dilution on tip opening and flame OH radical distribution of non-premixed Bunsen syngas mixture flames was investigated using OH-PLIF technique. The main results are summarized as follows:

Tip opening is evidently observed from the OH-PLIF images and the stretch rates are calculated accurately. Therefore, the phenomenon of the diffusion flame tip opening is caused by the negative

tensile action at the tip, where the stretching caused by the flow field inhomogeneity plays a leading role, and the curvature, which is the negative stretching effect caused by stretching, is negligible compared with the flow stretching.

As the V_{H2} in syngas increases, the mass diffusivity contributed by H_2 increases. As a result, the effect of mass diffusion is enhanced and the value of stretch rate decreases. Thus, the tip opening of laminar non-premixed Bunsen flames tend to be more evident. As the CO_2 dilution increases, V_{H2} in syngas decreases. Consequently, the chemical reaction residence time increases, the effect of mass diffusion is weakened, and the value of stretch rate increases. Therefore, the tip opening of laminar non-premixed Bunsen flames tend to be less evident.

As the V_{H2} in syngas increases and hydrogen content in syngas slightly increases, the total production rates of OH radicals slightly increase with a rate less than 7.5%. However, the profile of OH radical distribution becomes much broader. Thus, the maximum value of the OH radical counts reduces by 33.33%, 27.92%, and 23.09%, the OH radicals are more scattered, and the OH radical concentration decreases. As the CO_2 dilution increases, the production of OH radical is reduced due to the decrease in flame temperature. The percentage of fuel in syngas and the production rates of OH radicals decrease by approximately 20%. As a result, the maximum value of OH radical counts is reduced by 41.25%~49.7%, and the OH radical concentration decreases.

Acknowledgments:
The authors gratefully acknowledge financial support from Chongqing Science & Technology Commission [grant number CSTC2015shmszx90010].

Reference

[1] Tanksale A, Beltramini J N and Lu G Q M 2010 A review of catalytic hydrogen production processes from biomass *Renewable & Sustainable Energy Reviews* **14** 166-82
[2] Ansari M H, Jafarian S, Tavasoli A, Karimi A and Rashidi M 2014 Hydrogen rich gas production via nano-catalytic pyrolysis of bagasse in a dual bed reactor *Journal of Natural Gas Science & Engineering* **19** 279-86
[3] Blanco P H, Wu C and Williams P T 2014 Influence of Ni/SiO2 catalyst preparation methods on hydrogen production from the pyrolysis/reforming of refuse derived fuel *International Journal of Hydrogen Energy* **39** 5723-32
[4] Acharya B, Dutta A and Basu P 2010 An investigation into steam gasification of biomass for hydrogen enriched gas production in presence of CaO *International Journal of Hydrogen Energy* **35** 1582-9
[5] Phuhiran C, Takarada T and Chaiklangmuang S 2014 Hydrogen-rich gas from catalytic steam gasification of eucalyptus using nickel-loaded Thai brown coal char catalyst *International Journal of Hydrogen Energy* **39** 3649-56
[6] Cormos C C 2010 Evaluation of energy integration aspects for IGCC-based hydrogen and electricity co-production with carbon capture and storage *International Journal of Hydrogen Energy* **35** 7485-97
[7] Prathap C, Ray A and Ravi M R 2008 Investigation of nitrogen dilution effects on the laminar burning velocity and flame stability of syngas fuel at atmospheric condition *Combustion & Flame* **155** 145-60
[8] Pareja J, Burbano H J and Ogami Y 2010 Measurements of the laminar burning velocity of hydrogen–air premixed flames *International Journal of Hydrogen Energy* **35** 1812-8
[9] Kishore V R, Ravi M R and Ray A 2011 Adiabatic burning velocity and cellular flame characteristics of H 2 –CO–CO 2 –air mixtures *Combustion & Flame* **158** 2149-64
[10] Wang Z H, Weng W B, He Y, Li Z S and Cen K F 2015 Effect of H 2 /CO ratio and N 2 /CO 2 dilution rate on laminar burning velocity of syngas investigated by direct measurement and simulation *Fuel* **141** 285-92
[11] Burbano H J, Pareja J and Amell A A 2011 Laminar burning velocities and flame stability analysis

of H/CO/air mixtures with dilution of N and CO *International Journal of Hydrogen Energy* **36** 3232-42
[12] Paidi S K, Bhavaraju A, Akram M and Kumar S 2013 Effect of N 2 /CO 2 dilution on laminar burning velocity of H 2 –air mixtures at high temperatures *International Journal of Hydrogen Energy* **38** 13812-21
[13] Weng W B, Wang Z H, He Y, Whiddon R, Zhou Y J, Li Z and Cen K F 2015 Effect of N2/CO2 dilution on laminar burning velocity of H2–CO–O2 oxy-fuel premixed flame *International Journal of Hydrogen Energy* **40** 1203-11
[14] Makmool U, Jugjai S, Tia S, Laoonual Y, Vallikul P and Fungtammasan B 2011 Laser-based investigations of flow fields and OH distributions in impinging flames of domestic cooker-top burners *Fuel* **90** 1024-35
[15] Fu J, Tang C, Wu J and Huang Z 2014 Effect of preferential diffusion and flame stretch on flame structure and laminar burning velocity of syngas Bunsen flame using OH-PLIF *International Journal of Hydrogen Energy* **39** 12187-93
[16] Fu J, Tang C, Jin W, Thi L D, Huang Z and Zhang Y 2013 Study on laminar flame speed and flame structure of syngas with varied compositions using OH-PLIF and spectrograph *International Journal of Hydrogen Energy* **38** 1636-43
[17] Wang J, Wei Z, Yu S, Wu J, Xie Y, Zhang M and Huang Z 2015 Effects of stretch and preferential diffusion on tip opening of laminar premixed Bunsen flames of syngas/air mixtures *Fuel* **148** 1-8
[18] Vu T M, Min S C, Lee B J and Chung S H 2015 Tip opening of premixed bunsen flames: Extinction with negative stretch and local Karlovitz number *Combustion & Flame* **162** 1614-21
[19] Zhang B, Zhang L, Yang Z, Yan Y, Pu G and Guo M 2015 Hydrogen-rich gas production from wet biomass steam gasification with CaO/MgO *International Journal of Hydrogen Energy* **40** 8816-23
[20] Deniz I, Vardar-Sukan F, Yüksel M, Saglam M, Ballice L and Yesil-Celiktas O 2015 Hydrogen production from marine biomass by hydrothermal gasification *Energy Conversion & Management* **96** 124-30
[21] Gao N, Liu S, Han Y, Xing C and Li A 2015 Steam reforming of biomass tar for hydrogen production over NiO/ceramic foam catalyst *International Journal of Hydrogen Energy* **40** 7983-90
[22] Pu G, Huang B, Zhang X, Du J, Zhu T and Chen B 2018 Investigation of flame structure and burning intensity of partially premixed methane enrichment of syngas using OH-PLIF and kinetic simulation *Combustion Theory and Modelling* **22** 432-45